International Journal of Adhesion & Adhesives ▮ (▮▮▮▮) ▮▮▮–▮▮▮

Contents lists available at ScienceDirect

International Journal of Adhesion & Adhesives

journal homepage: www.elsevier.com/locate/ijadhadh

The selection and performance of adhesives for a steel–glass connection

M. Overend *, Q. Jin, J. Watson

Glass and Façade Technology Research Group, Department of Engineering, University of Cambridge, CB2 1PZ, UK

ARTICLE INFO

Article history:
Accepted 3 May 2011

Keywords:
Constitutive model
Glass
Steels
Finite element stress analysis
Viscoelasticity

ABSTRACT

Frame-supported glass structures such as curtain walls consist of glass infill plates mounted onto a framework of metallic elements. The longitudinal shear transfer at the interface of the glass and the metal is generally insufficient to mobilise composite action between the two materials, thereby making the units structurally inefficient. In this paper we investigate five candidate adhesives for load bearing steel–glass connections by means of mechanical testing and numerical modelling. The mechanical tests on representative steel–glass connections provide useful data for the selection of a suitable adhesive. The systematic characterisation of the time-dependent constitutive models of the bulk adhesives provides data essential for analytical and numerical models. Good agreement between the experimental results and the numerical models provides a basis for improving the structural efficiency of frame-supported glass structures.

1. Introduction

Over the last 30 years the use of large-area glazing in buildings has become increasingly popular. Applications range from curtain wall façade systems to glass floors and generally consist of glass infill panels mounted onto a subframe of metallic (steel or aluminium alloy) elements. More recently alternative mechanical and adhesive connections have been developed to enable a higher degree of transparency in glazing systems. These have been reviewed by Haldimann et al. [1].

The most popular mechanical connection, known as point fixing or point support, consists of a stainless steel bolt in a countersunk hole in the glass with an intermediate softer liner material (e.g. aluminium, POM or nylon) to reduce the bearing stresses. The glass in these applications is thermally treated to induce a surface precompression thereby increasing the tensile strength of glass that governs the design of these connections. The tensile strength of the glass, σ_f, shown in Eq. (1) is a function of the surface precompression resulting from the thermal strengthening of the glass, f_{rk}, that opposes the crack opening mode, and the inherent strength of material resulting from the depth of surface flaws, a.

$$\sigma_f = \frac{K_{IC}}{Y\sqrt{\pi a}} + f_{rk} \tag{1}$$

where K_{IC} is the plane strain fracture toughness ($0.72 \le K_{IC} \le 0.82$ MPa m$^{1/2}$ for soda lime silica glass) and Y is a geometry factor describing the crack geometry and the proximity of the specimen boundaries ($Y=1.12$ for straight plane edge cracks in a semi-infinite solid) [1,2]. Bolted glass connections are undesirable as the drilling process increases the depth of the stress raising flaws, a, in glass and it has been shown that the heat treatment process is less effective in the proximity of edges and holes leading to a reduction in, f_{rk} where the material is most highly stressed. The extent of the reduction in surface precompression is a function of the hole and plate geometry [3].

Adhesive connections provide an opportunity to overcome these deficiencies, but the only adhesive connection that has so far been widely accepted by the construction industry is elastomeric structural silicone glazing wherein factory-applied two-component silicones are used to bond the edges of the glass panels to steel or aluminium sub-frames [4–7]. Structural silicone joints are relatively thick (> 6 mm), low strength and flexible. They are therefore ideal for accommodating differential thermal strains between the glass and the metallic sub-frame, but are unsuitable for transferring the higher longitudinal shear required for composite action [8]. Recent investigations into the use of stiffer thermosetting adhesives for glass joints [8–12] show that it may be possible to develop a new generation of adhesive connections that outperform existing glass–metal connections, but there are three major gaps in this area: (1) a lack of data from standardised mechanical tests for a wide range of adhesives; (2) a paucity of information on the stress–strain characteristics of adhesives; (3) insufficient data on the long term performance of steel–glass adhesive joints.

It is therefore impossible to systematically select an adhesive and accurately size a connection for a steel–glass joint with an adequate degree of confidence. It is also not possible to undertake

* Corresponding author. Tel.: +44 1223 332659; fax: +44 1223 332662.
E-mail address: mo318@cam.ac.uk (M. Overend).

0143-7496/$ - see front matter © 2011 Elsevier Ltd. All rights reserved.
doi:10.1016/j.ijadhadh.2011.06.001

parametric design optimisation of adhesive joints such as that carried out for bolted glass connections [13,14]. This paper seeks to address points 1 and 2 above by investigating five candidate adhesives for steel–glass connections. The five commercial adhesives are first characterised by testing the bulk material leading to a definition of the visco-elastic plastic constitutive models of the adhesives. The mechanical performance of steel–glass adhesive connections is then investigated by mechanical tests on specially adapted single-lap shear (SLS) and T-peel specimens. The analytical calculations and numerical simulations of the adhesive joints are then described, followed by a discussion on the goodness-of-fit between these models and the experimental data. Finally, a basis for selecting adhesives for future steel–glass connections and recommendations for further testing are made.

2. Selection of the candidate adhesives

Due to the lack of guidelines on this particular application the selection of the five candidate adhesives was challenging and involved several consultations with adhesive manufacturers, glass manufacturers and other researchers. The selection criteria for the adhesives were that the adhesives: (1) were perceived to be especially suitable for a steel–glass connection; (2) represented a wide range of thickness, strength and stiffness; and (3) had a suitable viscosity and curing time to facilitate the assembly of the specimens in the laboratory. The five adhesives selected were:

- Dow Corning DC993 (silicone), a two-part silicone adhesive. Curing occurs by the polymerisation reaction that is triggered by the mixing of the two components that consist of a base compound (about 90% by volume) and a catalyst (about 10% by volume). Diffusion lengths among the two components are very small and curing progresses relatively quickly. This silicone adhesive is one of the leading products in the structural silicone glazing market.
- SikaForce 7550 L15 (polyurethane), a two-part polyurethane adhesive consisting of a thixotropic 2-component assembly adhesive, which cures by chemical reaction of a filled polyol-based resin (50% by volume) and an isocyanate-based hardener (50% by volume) to form a durable elastomer. This is a relatively new adhesive that has been specially developed for the façade industry.
- 3 M 2216B/A (epoxy), a two-part modified epoxy adhesive, which cures by the chemical reaction of a modified epoxy (40% by volume) and a modified amine (60% by volume). This two-part epoxy was reported to perform satisfactorily in glass–glass and glass–steel connections [9,15].
- Holdtite 3295 (2P-acrylic), a two-part acrylic adhesive, which cures by the chemical reaction of a methyl methacrylate resin (50% by volume) and an amine curing agent (50% by volume). This two-part acrylic was specially developed for glass applications and was reported to perform very well in a similar glass–steel test [15].
- Bohle 682-T (UV-acrylic), a UV-radiation cured acrylic adhesive based on a methylacrylate resin. This adhesive is used in glass–glass and glass–steel furniture and other internal applications.

3. Stress–strain behaviour of bulk adhesives

The stress–strain characteristics of the five candidate adhesives were expected to show strong time-dependence. It is also likely that some of these adhesives would exhibit hysteresis on cyclic loading [16,17], but this study concerned the performance of steel–glass joints to monotonically increasing strains and hence hysteresis is not investigated. The favoured approach for characterising the constitutive model of elastomers, is to decompose the stress–strain behaviour into an elastic component and a history-dependent component that describes the deviation from the elastic state [16–20]. The commercial Finite Element software LUSAS v14.3 was used for all the numerical modelling in this study. The visco-elastic model in LUSAS is based on Browning et al. [21] whereby the visco-elastic effects are restricted to the deviatoric component of the material response. This micromechanism inspired model (Fig. 1) therefore consists of two polymer networks acting in parallel: a time-independent elasto-plastic response and a time-dependent visco-elastic (Maxwell) response that represents the time-dependent deviation from equilibrium.

The visco-elastic material behaviour is therefore represented by a stress relaxation function

$$G(t) = G_v e^{-\beta t} \tag{2}$$

where G_v is the visco-elastic shear modulus and β is the decay constant.

In LUSAS the deviatoric visco-elastic stresses σ_v' at the current time t are obtained from the deviatoric strain rate $d\varepsilon'/ds$

$$\sigma_v'(t) = \int_0^t 2G(t-s)\frac{d\varepsilon'}{ds}ds \tag{3}$$

By substituting Eq. (2) into Eq. (3) it can be shown [22] that the deviatoric visco-elastic stresses at the updated position $(t+\Delta t)$ are

$$\sigma_v'(t+\Delta t) = \sigma_v'(t)e^{-\beta\Delta t} + 2G_v\frac{(1-e^{-\beta\Delta t})}{\beta}\frac{\Delta\varepsilon'}{\Delta t} \tag{4}$$

At each iteration these deviatoric visco-elastic stresses are added to the current elastic stresses. Furthermore, the assumption within LUSAS is that the visco-elastic stresses play no part in the yielding of the material. Consequently the visco-elastic stresses are stored separately and deducted from the total stress vector at each iteration prior to any plasticity computations. In this way stress states outside the yield surface are permissible, but after relaxation a state of stress reverts to that of the underlying elasto-plastic material. It was therefore necessary to decompose the mechanical response of the adhesives into: (1) time-dependent visco-elastic behaviour and (2) time-independent elasto-plastic behaviour. This was achieved by means of stress relaxation tests on uniaxially loaded adhesive dumbbells. The tests were conducted at 21 ± 2 °C on a computer-controlled Instron 5500 R electromechanical testing machine fitted with a 150 kN loadcell. The time-dependent visco-elastic properties were obtained from dumbbell tests, followed by transient load-relaxation tests on a second set of dumbbells to establish the time-independent elasto-plastic properties.

3.1. Adhesive dumbbell preparation

Dumbbells largely conforming to BS EN ISO 527-1 [23] and BS EN ISO 527 [24] were prepared by casting the adhesives into a silicone rubber mould and out-gassed to remove air bubbles (Fig. 2). All the dumbbells were 4 mm thick apart from the 2P-acrylic and the UV-acrylic dumbbells. The latter were cured

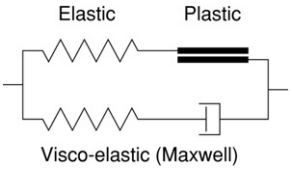

Fig. 1. One-dimensional representation of the constitutive model.

Please cite this article as: Overend M, et al. The selection and performance of adhesives for a steel–glass connection. Int J Adhes Adhes (2011), doi:10.1016/j.ijadhadh.2011.06.001

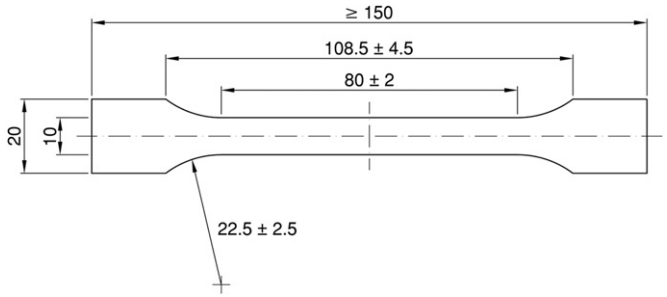

Fig. 2. Dumbbell geometry [23].

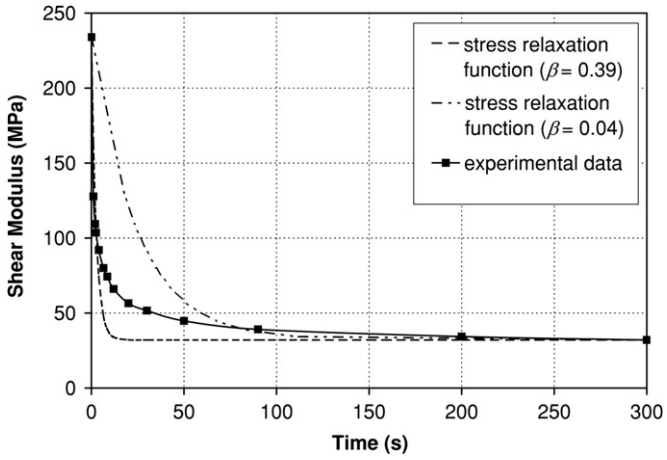

Fig. 3. Shear modulus vs. time relationship for epoxy dumbbell.

in 3 layers to a total thickness of 1 mm thereby ensuring penetration of the UV-radiation. In an attempt to reduce the number of air bubbles, the thickness of the 2P-acrylic dumbbells was reduced to 1 mm, but this was not entirely successful, resulting in relatively poor quality 2P-acrylic dumbbells.

3.2. Experimental determination of visco-elastic properties

The visco-elastic properties of the adhesives were obtained by applying an instantaneous uniform tension to the dumbbells up to a predefined strain, followed by a holding period during which stress relaxation was recorded. In practice viscous energy is dissipated during the brief initial straining period. A procedure for correcting the experimental data was therefore devised and is described elsewhere for brevity [25]. The corrected stress vs. time response was converted into shear modulus vs. time $G(t)$ relationship from

$$G(t) = \frac{\sigma(t)}{2(1+\nu)\varepsilon(t)} \tag{5}$$

where $\sigma(t)$ and $\varepsilon(t)$ are the corrected stress vs. time and strain vs. time responses obtained from the experimental investigations and ν is the Poisson's ratio obtained from the manufacturers' data and verified experimentally. The visco-elastic shear modulus G_v was obtained by subtracting the residual shear modulus, G_∞, from the initial shear modulus (Fig. 3).

The decay constant β was obtained by curve fitting the stress relaxation function (Eq. (2)) to the experimental data. This may either be obtained by minimising the sum of the square differences of the shear modulus ($M1$) or by minimising the sum of square differences of the time ($M2$), leading to an underestimation of the decay period and an overestimation of the adhesive stiffness, respectively (Fig. 3). The resulting visco-elastic properties are summarised in Table 1.

Table 1
Visco-elastic properties of adhesives.

	Poisson's ratio, ν	Shear modulus, G_v (MPa)	Decay time, t_d (s)	Decay constant, β	
				M1	*M2*
Silicone	0.49	0.03	121	1.23	1.3
Polyurethane	0.39	1.50	92	0.77	0.75
Epoxy	0.46	201.88	502	0.39	0.04
2P-acrylic	0.39	195.89	1065	0.087	0.075
UV-acrylic	0.30	386.23	1373	0.022	0.007

3.3. Experimental determination of elasto-plastic properties

The elasto-plastic properties were determined experimentally by transient stress relaxation tests on five dumbbells per adhesive. The dumbbells were loaded in five or more increments up to failure. Each increment consisted of a loading period at a rate of 66.6 N s^{-1} followed by a holding period t_d obtained from the preceding visco-elastic property tests (Table 1).

The decay points at the end of each holding period (Fig. 4b), therefore represent the time-independent stress in the adhesive for the corresponding strain (Fig. 4a). Expressions for the elasto-plastic stress–strain relationship were then obtained by polynomial curve fitting to these decay points (Fig. 4c) and are shown in Table 2.

3.4. Summary of the bulk material properties

The two methods used to determine the decay constant, β, (i.e. *M1* and *M2*) produce comparable values for the silicone, polyurethane and 2P-acrylic tested, but significantly different values for the epoxy and the UV-cured adhesives. These discrepancies suggest that the visco-elastic relationship in Eq. (2) provides a good description of the mechanical response of the former, but not the latter adhesives.

Fig. 4 reveals that despite keeping the same holding time, t_d, the percentage decay of stress seems to decrease as the test progresses through the load increments of the stress relaxation tests. This phenomenon was observed in all the adhesives tested and suggests nonlinear visco-plastic behaviour where the shear modulus is a function of both time and stress. This was not investigated further in this study.

In all five of the adhesives tested, 50% of the stress relaxation occurred in the initial 0.9–1.7% of t_d (i.e. 0.5–17.0 s) and 90% of the relaxation was observed within 1.9–50.0% of t_d (i.e. 1.0–500.0 s). The visco-elastic characteristics are therefore negligible for low strain rates (e.g. self weight, permanent superimposed loads, snow loads, etc.), but may be significant for higher strain rates (such as impact, wind and blast induced pressures).

4. Mechanical testing of steel–glass adhesive joints

The aim of these tests was to determine the load bearing characteristics of the five candidate adhesives in close-to-reality steel–glass joints. The test assemblies shown in Fig. 5 consisted of single-lap shear (SLS) tests based on ASTM D1002 [26] and T-peel tests adapted from the ASTM D1876 guidelines [27]. The bonding area of all steel–glass joints was 50.8 mm wide by 26 mm long (lap-length) with a tolerance of ±1 mm. All specimens were made from two identical 6.35 mm thick bright mild steel

Please cite this article as: Overend M, et al. The selection and performance of adhesives for a steel–glass connection. Int J Adhes Adhes (2011), doi:10.1016/j.ijadhadh.2011.06.001

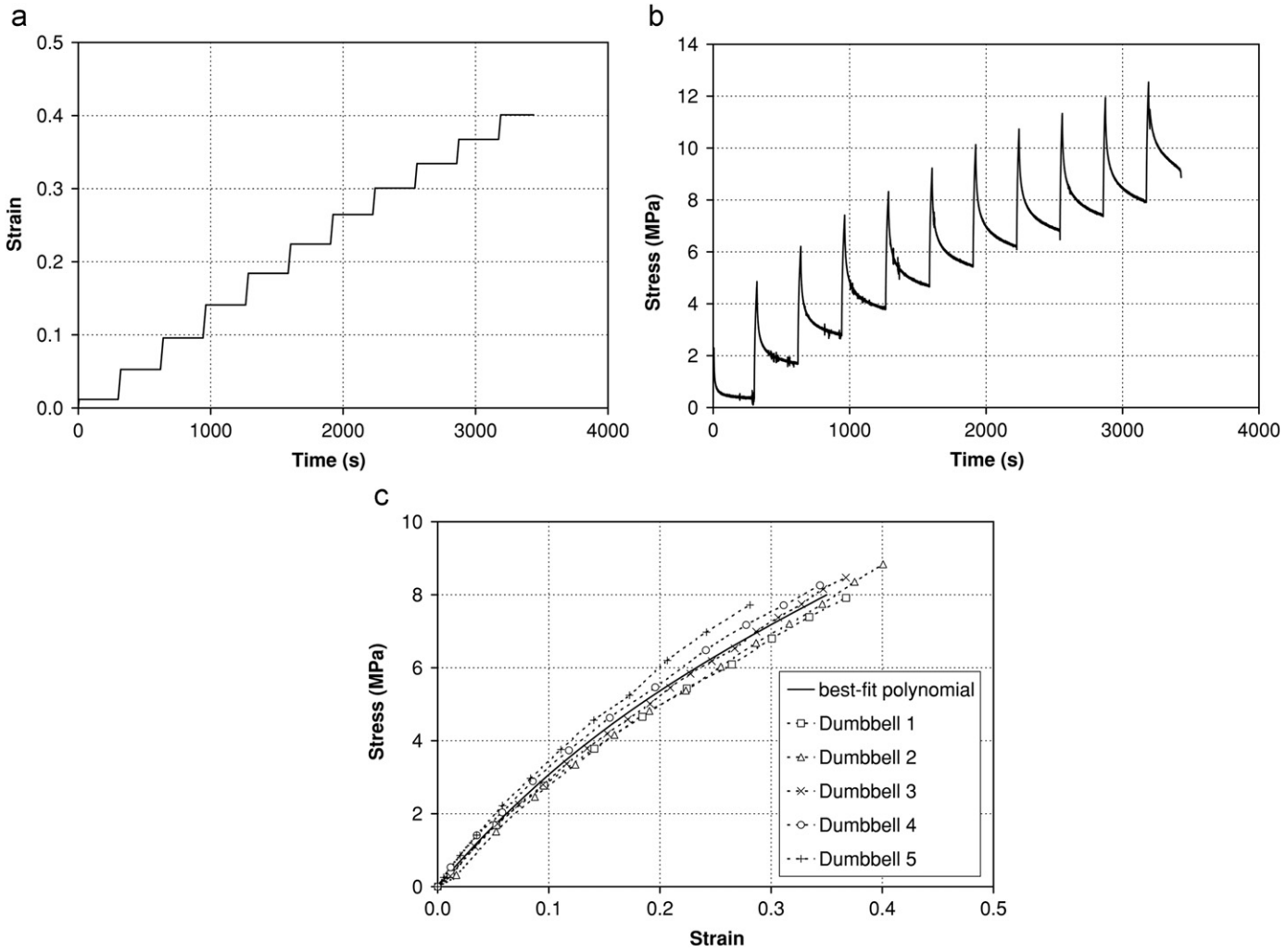

Fig. 4. Time-independent response of epoxy dumbbell: (a) typical strain history, (b) typical stress vs. time; response and (c) curve fitting to stress vs. strain experimental data obtained from five dumbbells.

Table 2
Time-independent elasto-plastic stress–strain polynomials.

	Elasto-plastic stress–strain polynomial	R^2-value	Mean failure strain
Silicone	$\sigma = 0.311\varepsilon^3 - 1.0691\varepsilon^2 + 1.8825\varepsilon$	0.9943	1.33
Polyurethane	$\sigma = -9.2036\varepsilon^4 + 20.985\varepsilon^3 - 18.455\varepsilon^2 + 10.23\varepsilon$	0.9997	1.06
Epoxy	$\sigma = 49.037\varepsilon^3 - 53.513\varepsilon^2 + 35.575\varepsilon$	0.9858	0.35
2P-acrylic	$\sigma = 1142.312\varepsilon$, for $0 \le \varepsilon \le 0.00135$; $\sigma = 227681\varepsilon^3 - 13587\varepsilon^2 + 324.95\varepsilon + 1.1255$ for $\varepsilon > 0.00135$	0.9132	0.0265
UV-acrylic	$\sigma = -2336.4\varepsilon^3 - 705.81\varepsilon^2 + 53.499\varepsilon$ for $0 \le \varepsilon \le 0.032$; $\sigma = 9.127$ for $0.032 \le \varepsilon \le 0.043$	0.9196	0.0430

elements conforming to BS EN 10277-2 [28] and a 10 mm thick fully toughened glass plate manufactured to BS EN 12150-2 [29]. A total of fifty specimens were tested comprising of 5 specimens $\times 5$ adhesives $\times 2$ test assemblies.

4.1. Surface preparation

The surfaces of the steel adherends were left unabraded for the silicone and the polyurethane. Steel surfaces were sanded with 180 grade sandpaper in preparation for the epoxy and 2P-acrylic adhesives. The steel surfaces intended for the UV-acrylic were ground. Table 3 shows the roughness measured with a Talysurf 120 stylus profiler. All surfaces were cleaned with a universal cleaning agent to remove foreign matter and contaminants. In addition, a solvent-based activator and a pigmented solvent-based polyisocyanate primer recommended by the manufacturer were applied to the polyurethane adherends. A manufacturer-recommended siloxane based primer was applied to the steel adherends for the silicone joints.

4.2. Sample assembly

The five adhesives had different mixing requirements. The 2P-acrylic and the epoxy were mixed thoroughly by hand in

Please cite this article as: Overend M, et al. The selection and performance of adhesives for a steel–glass connection. Int J Adhes Adhes (2011), doi:10.1016/j.ijadhadh.2011.06.001

a measuring cylinder. The silicone and the polyurethane required proprietary mixing equipment consisting of a static mixer attached to a pneumatic dispenser for the polyurethane and a cork-screw fitting attached to an electric drill for the silicone. The UV-acrylic is a single component adhesive and had no mixing requirements. Misalignment during assembly was minimised by placing the steel and glass adherends into CNC cut assembly jigs. The optimal thickness of the adhesives varied considerably from 6 mm for silicone to 0.106 mm for UV-acrylic (Table 4). Glass microspheres mixed with the adhesive were used to provide the specified thickness in sub-millimetre adhesives. Glass shims cut from 3 mm thick glass provided the required bond thickness for the silicone and the polyurethane.

All the adhesive specimens other than the UV-acrylic were cured by storing the specimens at a temperature of 22 ± 2 °C and a relative humidity of $40 \pm 5\%$. The UV-acrylic specimens were cured for 60 s under a high intensity UV light (300 W Osram Ultra-Vitalux) at a distance of 100 mm. Manufacturer recommendations on handling and curing times, shown in Table 4, were adopted for all adhesives. All adhesives were tested within 24 h of curing.

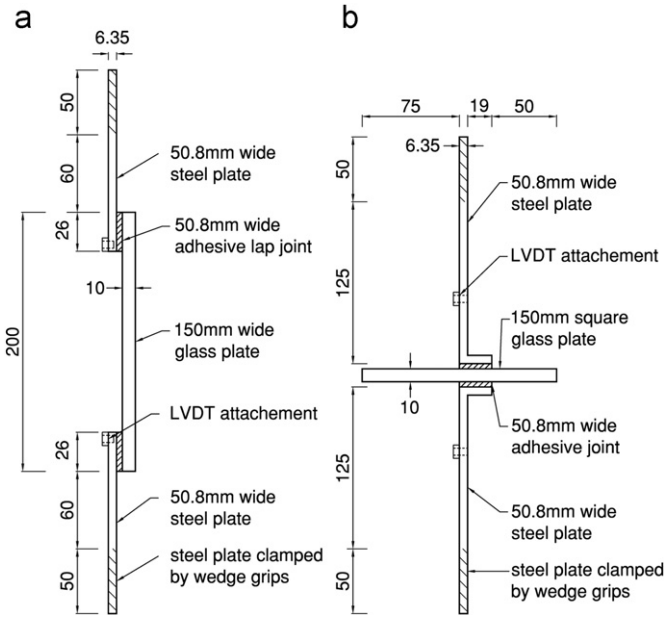

Fig. 5. Test specimens: (a) single-lap shear (SLS) and (b) T-peel.

Table 3
Surface roughness of steel adherends.

	R_a[a] (μm)	R_q[b] (μm)	Maximum deviation from mean (μm)
Unabraded steel	4.97	6.27	24.42
Sanded steel	0.47	0.66	4.91
Ground steel	0.2	0.27	1.60

[a] R_a is the arithmetic average of the absolute vertical deviations from the mean.

[b] R_q is the root mean square of the absolute vertical deviations from the mean.

4.3. Test apparatus and procedure

The tests were performed on a computer-controlled Instron 5500R electromechanical testing machine fitted with a 150 kN loadcell and mechanical wedge action grips (Fig. 6). In-plane and lateral displacements were measured by means of linear variable differential transformers (LVDTs) and recorded on a Solartron SI 3535D Scorpio datalogging system. The tests were conducted to controlled crosshead speeds shown in Table 4. The rates selected were chosen to limit test durations to less than 20 min.

4.4. Test results and observations

A summary of the results is shown in Table 5 and load-displacement results are plotted in Fig. 11. Furthermore, the failed specimens were examined with the naked eye. Cohesive failure in the adhesive phase was observed in all the silicone adhesive tests (Fig. 7a). All the polyurethane samples, other than three of the SLS samples, failed in adhesion at the primer and polyurethane interface closer to the steel surface (Fig. 7b). The epoxy SLS samples failed cohesively in the adhesive phase, whereas the epoxy T-peel samples all failed in adhesion partly at the adhesive–steel interface and partly at the adhesive–glass interface (Fig. 7c). The UV-acrylic and 2P-acrylic T-peel specimens failed cohesively in the adhesive phase as expected. Glass failure was observed in four of the five SLS specimens of both the UV-acrylic and the 2P-acrylic adhesives. In all glass failure cases the origin of failure was located close to the edge of the adhesive joint (Fig. 7d). The remaining SLS specimens failed cohesively in the adhesive phase. Discolouration (whitening) was observed for the UV-acrylic and 2P-acrylic SLS specimens, this first appeared towards the edges of the lap-joint and progressed towards the central areas with increasing load.

5. Analytical and numerical predictions and validation with experimental data

This section describes the existing analytical methods and nonlinear FE analysis that were used to simulate the performance of steel–glass joints and the validation of these models with the experimental data obtained from Section 4.

5.1. Analytical methods

The existing analytical models for predicting the complex stress state in single-lap joints are often based on simplifications that are necessary for arriving at a solution [30]. For example,

Table 4
Specimen preparation and crosshead speed.

	Handling time (h)	Curing time (h)	Surface roughness		Bond thickness (mm)	Crosshead speed	
			R_a (μm)	R_q (μm)		SLS (mm/min)	T-peel (mm/min)
Silicone	24.0	168.0	4.97	6.27	6.0	2.0	2.0
Polyurethane	1.0	3.0	4.97	6.27	3.0	2.0	1.0
Epoxy	12.0	7.0	0.47	0.66	0.212	0.1	0.1
2P-acrylic	0.05	0.08	0.47	0.66	0.106	0.18	0.1
UV-acrylic	0.01	0.01	0.20	0.30	0.106	0.1	0.1

Please cite this article as: Overend M, et al. The selection and performance of adhesives for a steel–glass connection. Int J Adhes Adhes (2011), doi:10.1016/j.ijadhadh.2011.06.001

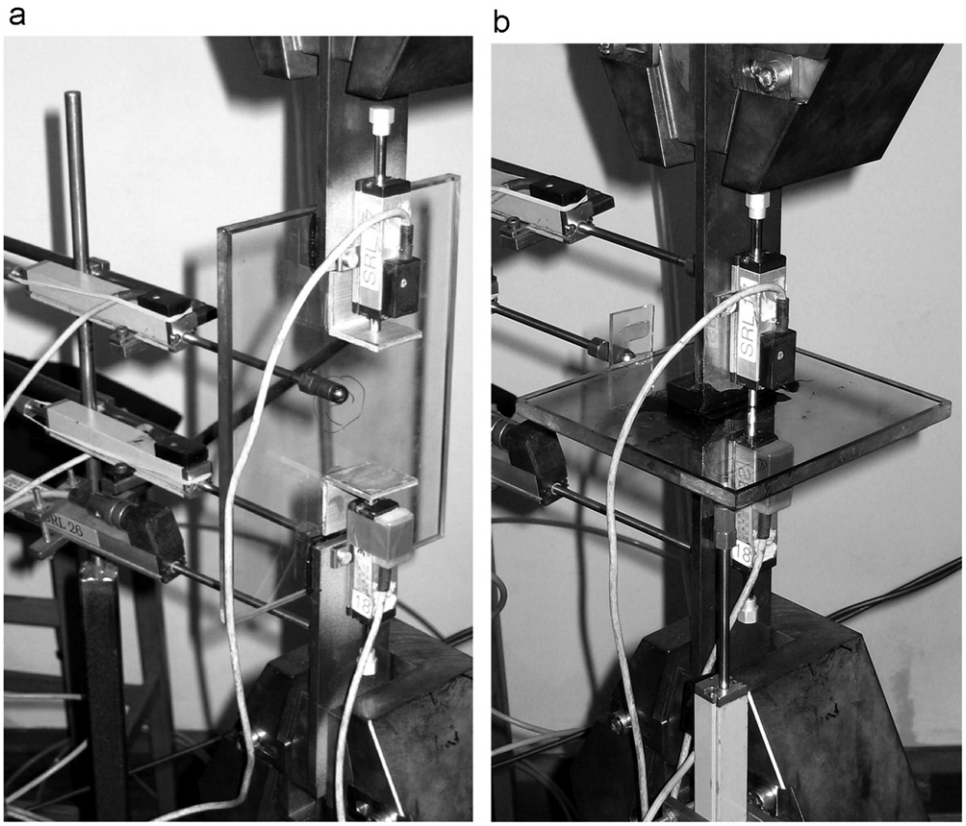

Fig. 6. Test setup for (a) single-lap shear test and (b) T-peel test.

Table 5
Summary of test results.

	Test type	Mean failure load (kN)	Mean extension at failure load (mm)	Mean time to failure (s)	Coefficient of variation of failure load
Silicone	SLS	0.795	7.828	432.8	0.065
	T-peel	1.356	2.450	109.2	0.105
Polyurethane	SLS	1.335	1.81	133.6	0.484
	T-peel	1.244	0.414	29.8	0.205
Epoxy	SLS	9.019	0.282	355.8	0.094
	T-peel	4.529	0.108	149.6	0.413
2P-acrylic	SLS	19.123[a]	0.550	362.4	0.081
	T-peel	9.484	0.362	302.0	0.069
UV-acrylic	SLS	13.482[a]	0.096	774.8	0.396
	T-peel	13.417	0.064	622.0	0.077

[a] Glass failure in 4 out of 5 specimens.

Her [31] and Tsai et al. [32] provide approximate equations for determining the stresses in an adhesive with dissimilar adherends, both of them, however, ignore bending. The most suitable method for this application is that of Bigwood and Crocombe [33] that can be performed through a spreadsheet and gives the shear and peel stresses in the adhesive. A drawback of this method is that it requires knowledge of the loading conditions at the ends of the overlap region rather than at the ends of the adherends. Another limitation is that this method adopts linear elastic models for both adhesive and adherends.

5.2. Numerical models

A 2-dimensional FE model was constructed for each test type using LUSAS v14.3 on a Windows-based PC with a 2.83 GHz processor and 7.93 GB of RAM. Since the adhesive width (50.8 mm) of the sample was large compared to the adhesive thickness (0.106–6 mm), strain across the width was considered to be negligible and quadrilateral quadratic 8-noded plane strain elements with visco-elastic and elasto-plastic modelling capabilities were used throughout.

Half of each connection was modelled due to symmetry (Figs. 8 and 9). The boundary conditions were δ_x and M_z restraints along the line of symmetry *AB* and δ_y and M_z restraints along the 50 mm grip length *CD* and *EF*. Visco-elastic and elasto-plastic properties of the adhesives were obtained from Tables 1 and 2, respectively. The adherends were modelled as linear perfectly elastic ($E_{steel}=209$ GPa, $v_{steel}=0.3$, $E_{glass}=70$ GPa, $v_{glass}=0.22$).

Convergence testing by *h*-refinement of a typical SLS joint revealed that coarse meshes tended to underestimate the stress

Please cite this article as: Overend M, et al. The selection and performance of adhesives for a steel–glass connection. Int J Adhes Adhes (2011), doi:10.1016/j.ijadhadh.2011.06.001

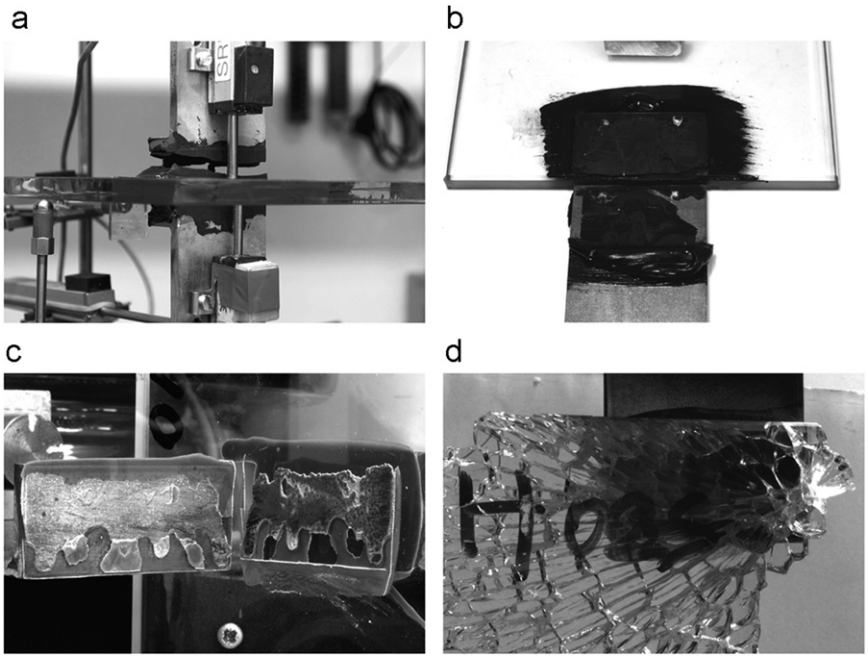

Fig. 7. Typical failure modes showing (a) cohesive failure in the silicone phase, (b) adhesion failure at the primer and polyurethane interface, (c) interfacial failure in epoxy T-peel test and (d) glass failure in 2P-acrylic test.

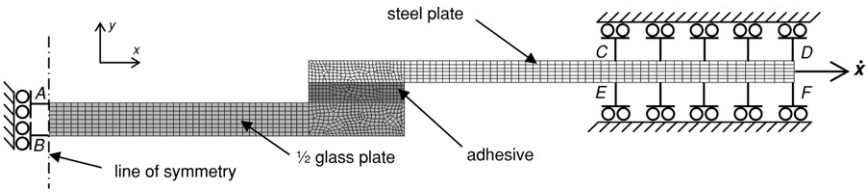

Fig. 8. FE model of silicone SLS connection. Boundary conditions and load shown schematically. Adhesive mesh consists of 6×26 divisions.

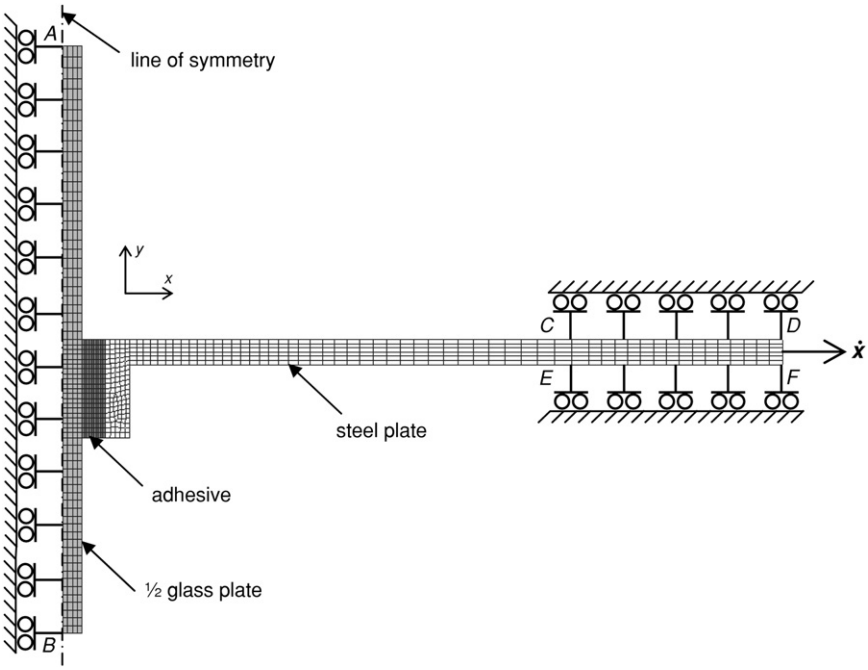

Fig. 9. FE model of silicone T-peel connection. Boundary conditions and load shown schematically. Adhesive mesh consists of 10×20 divisions.

concentrations at the edge of the adhesive. The adhesive thickness was therefore modelled using sufficiently dense meshes i.e. 4 to 6 elements in thickness, and an element aspect ratio < 10.

A displacement rate was applied to the end of the steel plate corresponding to half the experimental crosshead speed shown in Table 4. The total response time of the nonlinear transient

analysis was determined from the experimental data shown in Table 5. The dynamic analysis was performed using the implicit method and an updated Lagrangian approach was selected to capture geometric nonlinearity and material nonlinearity whilst preventing mesh penetration. The convergence criteria for each time step were set as follows: (a) the residual force norm ≤ 0.1; (b) the incremental displacement norm ≤ 1; and (c) the number of iterations ≤ 12.

The analysis failed to converge when one of the highly stressed elements located towards the ends of the lap-joint had reached the failure strain shown in Fig. 4c, and was therefore unable to redistribute the load to the other regions of the adhesive, thereby underestimating the load bearing capacity of the adhesive joint. This was overcome by means of an element deactivation strategy, whereby the elements with the highest principle stress were deactivated manually when the iteration failed to converge. In doing so the deactivated elements remain in the solution with a stiffness of zero and represent the complete failure of the corresponding part of the material.

In addition to the nonlinear analyses described above, a linear elastic analysis was also performed to provide a like-for-like comparison with the linear elastic analytical methods described in Section 5.1. The Young's modulus for the linear analysis $E_{adhesive}$ was obtained from the slope of the initial stage of the time-independent elasto-plastic responses in Table 2.

5.3. Numerical results and validation

The shear stresses obtained from the nonlinear (visco-elastic plastic) FE analysis and the linear elastic analytical solutions plotted in Fig. 10 are generally in good agreement, with the exception of the stress concentration regions close to the edges of the adhesive, where the analytical models tend to underestimate the magnitude of the shear stresses. The relative differences between nonlinear FE analysis and the analytical solution remain constant ($\leq 10\%$) with increasing load up to the point of failure, beyond which the agreement between the two solutions becomes progressively poorer. This is due to the deactivation of the elements at the extremities of the lap-joint as they reach the failure strain, leading to a redistribution of stresses onto a smaller length of adhesive.

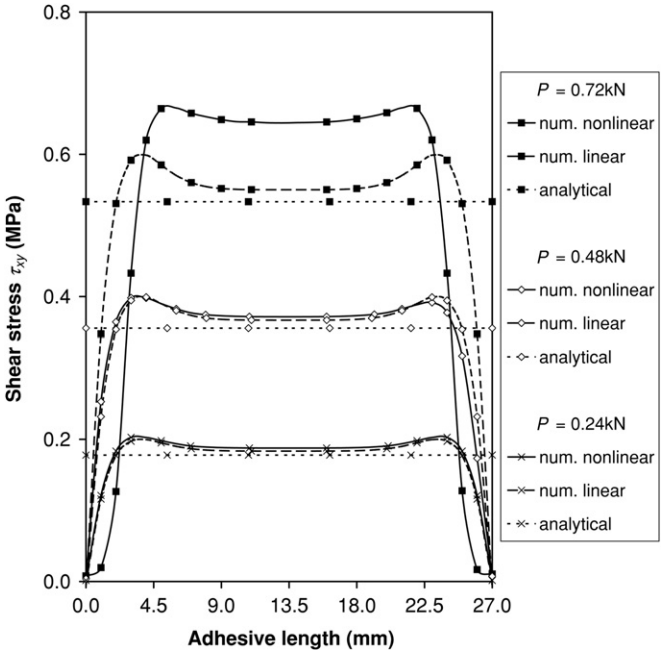

Fig. 10. Analytical and numerical shear stresses at mid-depth of the silicone adhesive joint with reaction $P=0.24$, 0.48 and 0.72 kN.

The visco-elastic plastic numerical solution and the linear elastic numerical solution show excellent agreement at low strains, but substantial differences at higher strains. The former is due to the limited plasticity of the adhesive at low loads and the relatively low strain rates that reduce the influence of viscoelasticity. The latter is caused by the plastic deformation of the adhesive and the afore-mentioned deactivation of the elements in the highly stressed edge regions of the adhesive.

Stress contour plots obtained from the nonlinear FE analysis are not shown here for brevity, but reveal that the bulk of the adhesive in the SLS is subjected to a relatively uniform shear stress, which increases rapidly toward the ends of the adhesive joint as expected. The principal stresses observed in the T-peel numerical analysis are also as expected with substantial lateral deformations in the adhesives due to Poisson's ratio effects. This corresponds to the deformations observed in the experimental investigations.

The principal stress concentrations on the surface of the glass of the UV-acrylic and the 2P-acrylic SLS joints are of particular interest due to the glass failure observed in the experimental investigations. The maximum principal stress on the glass surface obtained from the FE analysis is 109.3 MPa when the reaction $P=9.01$ kN. This is approximately the stress at which fully toughened glass is expected to fail.

The load vs. displacement results in Fig. 11 show that the best agreement between experimental and numerical results was obtained in the silicone SLS, the silicone T-peel and for the stronger SLS polyurethane specimens that failed in cohesion. There is a moderate agreement for the SLS epoxy and poor agreement for the other adhesives. This is generally expected as the accuracy of the numerical model is contingent on two main factors:

(1) The accuracy of the bulk adhesive properties obtained from the dumbbell tests. This is illustrated by the poor numerical models arising from difficulties in preparing good quality dumbbells for the UV-acrylic (Fig. 11i and j) and particularly the 2P-acrylic (Fig. 11g and h) where the fit is very poor and has been omitted for clarity. The moderate agreement for the SLS epoxy (Fig. 11e) is a result of the inaccurate constitutive model shown in Fig. 3.
(2) The cohesive failure of the test specimens. This is illustrated by the overestimation of the joint strength in the polyurethane T-peel (Fig. 11d) and the epoxy T-peel (Fig. 11f) both of which failed in adhesion. Likewise, the variability in strength of the UV-acrylic (Fig. 11i and j) was difficult to predict as the failure of the joint was governed by glass failure.

6. Conclusions

The principal objective of this study was to identify adhesives suitable for load bearing steel–glass connections. This objective was achieved by investigating the mechanical performance of five candidate adhesives. Table 6 provides quantitative and qualitative information that is useful for initial adhesive selection. This table suggests that, for the adhesives geometries tested, the mean shear strength is inversely proportional to the thickness of the adhesive joint.

From Table 6 it may be concluded that the best adhesive for a low strength/low stiffness steel–glass joint is the silicone. In the event that a stiffer and/or stronger joint is required the two adhesives to consider are the 2P-acrylic and the epoxy. These

Please cite this article as: Overend M, et al. The selection and performance of adhesives for a steel–glass connection. Int J Adhes Adhes (2011), doi:10.1016/j.ijadhadh.2011.06.001

recommendations are, however, based on the adhesives' performance under short duration loads in a laboratory environment. Further research on the performance of these adhesives when subjected to close-to-reality actions such as long duration loading, cyclic loading and aggressive environments, is therefore required to determine their long-term mechanical performance.

The second objective of this study was to identify and validate a methodology for sizing steel–glass adhesive connections. It has been shown that nonlinear transient FE analysis can provide very good predictions of mechanical performance, but this is contingent on the accuracy of the bulk material properties of the adhesive and in particular on the successful decoupling of the time-dependent visco-elastic behaviour from the time-independent elasto-plastic response. This is a relatively laborious process and one that requires carefully controlled stress relaxation tests on good quality dumbbells. It, however, has an

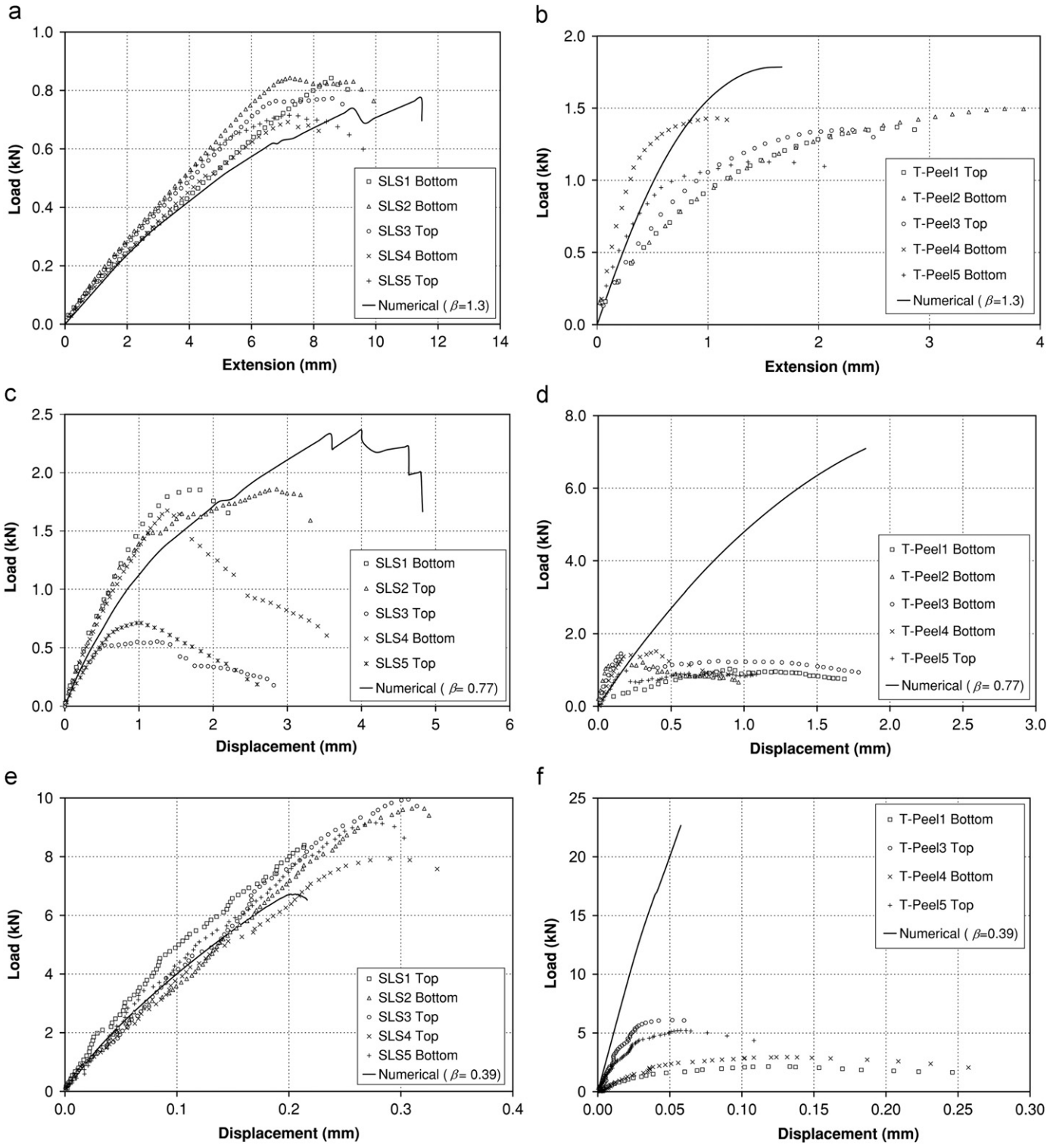

Fig. 11. Load vs. displacement results from experimental tests and numerical analysis for (a) SLS silicone, (b)T-peel silicone, (c) SLS polyurethane, (d) T-peel polyurethane, (e) SLS epoxy, (f) T-peel epoxy, (g) SLS 2P-acrylic, (h) T-peel 2P-acrylic, (i) SLS UV-acrylic and (j) T-peel UV-acrylic.

Please cite this article as: Overend M, et al. The selection and performance of adhesives for a steel–glass connection. Int J Adhes Adhes (2011), doi:10.1016/j.ijadhadh.2011.06.001

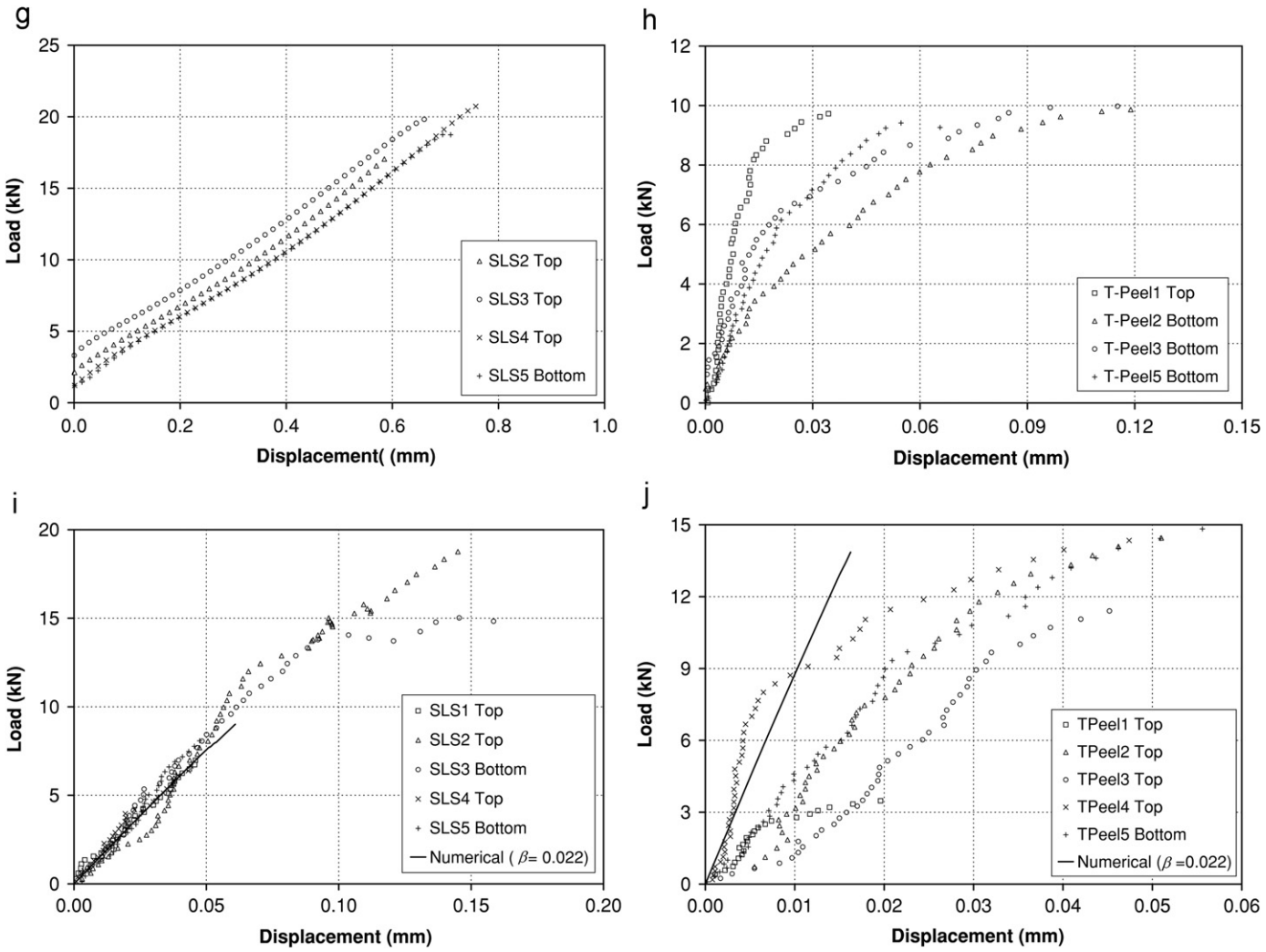

Fig. 11. (*continued*)

Table 6
Adhesive selection table.

	Mean shear strength [a] (MPa)	Visco-elastic shear modulus G_v (MPa)	Residual shear modulus G_∞ (MPa)	Mean pull-out strength [c] (MPa)	Ductility	Ease of preparation and tooling	Strength variability[d]
Silicone	0.58	0.03	0.55	1.07	High	Med.	Low
Polyurethane	0.97	1.50	2.09	0.98	High	Low	High
Epoxy	7.21	201.88	32.10	3.57	Med.	High	Med.
2P-acrylic	15.30[b]	195.89	161 .00	7.47	Low	High	Low
UV-acrylic	9.83[b]	386.23	347.81	10.56	V. low	Med.	Med.

[a] Based on short term loading and equivalent constant shear stress along the 26 mm long SLS joint.
[b] Governed by glass failure.
[c] Based on short term loading and equivalent constant tensile stress across the T-peel joint.
[d] Based on SLS and T-peel joints.

important practical significance in that the apparent stiffness, and hence the magnitude of the stress concentrations on the glass surface, is very sensitive to the applied strain rate. Further research in this field is required to characterise the hysteretic response of the adhesives to cyclic loads, to devise more accurate constitutive models that capture the nonlinear visco-plastic response of the adhesives and to provide an automated and consistent procedure for deactivating elements in the FE analysis.

References

[1] Haldimann M, Luible A, Overend M. Structural use of glass. Structural engineering document SED10. International Association for Bridge and Structural Engineering IABSE, Zürich; May 2008.
[2] Lawn B. Fracture of brittle solids, second ed. Cambridge University Press, 1993.
[3] Nielsen JH, Olesen JF, Poulsen PN, Stang H. Simulation of residual stresses at holes in tempered glass: a parametric study. Materials and Structures 2009; 43(7):947–61.

Please cite this article as: Overend M, et al. The selection and performance of adhesives for a steel–glass connection. Int J Adhes Adhes (2011), doi:10.1016/j.ijadhadh.2011.06.001

[4] EOTA. Structural sealant glazing systems—SSGS. ETAG Nr. 002 (July 1998). EOTA—European Organisation for Technical Approvals, Brussels; 1998.
[5] CSTB 3488. Vitrages extérieurs collés—Cahier des prescriptions techniques. Cahier du CSTB, Livraison 444, Cahier 3488; November 2003.
[6] AAMA CW-13-85. AAMA CW-13-85: structural sealant glazing systems. American Architectural Manufacturers Association (AAMA), Schaumburg, USA; 1985.
[7] ASTM C 1401-02. Standard guide for structural sealant glazing. American Society for Testing Materials; 2002.
[8] Mocibob D, Crisinel M. Linear connection system for structural application of glass panels in fully-transparent pavilions. Challenging Glass. Delft, Netherlands; 2008.
[9] Pye A, Ledbetter S. The selection of an adhesive for a glass–adhesive T-beam. International Journal of Adhesion and Adhesives 1998;18:159–65.
[10] Wellershoff F, Sedlacek G. Glued connections for new steel glass structures. In: Proceedings of the Glass Processing Days, Tampere, Finland; 2005.
[11] Louter C, Veer F, Hobbelman G. Reinforcing glass, effects of reinforcement geometry and bonding technology. In: Proceedings of the Glass Performance Days, Tampere, Finland; 2007, p. 93–7.
[12] Weller B, Schadow T. Designing of bonded joints in glass structures. In: Proceedings of the Glass Performance Days, Tampere, Finland; 2007, p. 74–6.
[13] Overend M. Optimising connections in structural glass. In: Proceedings of the Glass in Buildings 2, Bath, UK; 2005, p. 7–8.
[14] Bernard B, Daudeville F. Point fixings in annealed and tempered glass structures: modelling and optimization of bolted connections. Engineering Structures 2009;31(4):946–55.
[15] Overend M. The appraisal of structural glass assemblies. PhD Thesis, University of Surrey, UK; March 2002.
[16] Bergstrom JS, Boyce MC. Constitutive modelling of the large strain time-dependent behaviour of elastomers. Journal of Mechanics and Physics of Solids 1998;46(5):931–54.
[17] Qi HJ, Boyce MC. Stress–strain behaviour of thermoplastic polyurethanes. Mechanics of Materials 2005;37(8):817–39.
[18] Green MS, Tobolsky AV. A new approach to the theory of relaxing polymeric media. Journal of Chemical Physics 1946;14(2):80–92.
[19] Johnson AR, Quigley CJ. A viscohyperelastic maxwell model for rubber viscoelasticity. Rubber Chemistry and Technology 1992;65:137–53.
[20] Roland CM. Network recovery from uniaxial tension in elastic equilibrium. Rubber Chemistry and Technology 1989;62:863–79.
[21] Browning RV, Gurtin ME, Williams WO. A one-dimensional viscoplastic constitutive theory for filled polymers, Int. Journal of Solids and Structures 1984;20(11/12):921–34.
[22] LUSAS Finite Element System. LUSAS Theory Manual. FEA Ltd., UK; 2010.
[23] BS EN ISO 527-1:1996. Plastics—determination of tensile properties—part 1: general principles. British Standards Institution; 1996, p. 1–16.
[24] BS EN ISO 527-2:1996. Plastics—determination of tensile properties—part 2: test conditions for moulding and extrusion plastics. British Standards Institution; 1996, p. 1–14.
[25] Overend M, Jin Q, Watson JK. Investigations into steel–glass adhesive joints. Technical report CUED/D-Struct/TR231. Department of Engineering University of Cambridge; June 2010.
[26] ASTM D 1002-99 standard test method for apparent shear strength of single-lap-joint adhesively bonded metal specimens by tension loading (metal-to-metal). ASTM Standards; 1999.
[27] ASTM D 1876-93 standard test method for peel resistance of adhesives (T-peel test). ASTM Standards; 1993.
[28] BS EN 10277-5:2008. Bright steel products. Technical delivery conditions. Steels for quenching and tempering. British Standards Institution; 2008, p. 1–16.
[29] BS EN 12150-2:2004. Glass in building. Thermally toughened soda lime silicate safety glass. Evaluation of conformity/product standard, British Standards Institution; 2004, p. 1–42.
[30] Adams RD, editor. Adhesive Bonding. Cambridge, UK: Woodhead Publishing Limited; 2005.
[31] Her S. Stress analysis of adhesively-bonded lap joints. Composite Structures 1999;47:673–8.
[32] Tsai MY, Oplinger DW, Morton J. Improved theoretical solutions for adhesive lap joints. International Journal of Solids and Structures 1998;35:1163–85.
[33] Bigwood DA, Crocombe AD. Elastic analysis and engineering design formulae for bonded joints. International Journal of Adhesion and Adhesives 1989; 9:229–42.

Please cite this article as: Overend M, et al. The selection and performance of adhesives for a steel–glass connection. Int J Adhes Adhes (2011), doi:10.1016/j.ijadhadh.2011.06.001